A Stochastic Parameter Perturbation Method to Represent Uncertainty in a Microphysics Scheme

GREGORY THOMPSON,[a] JUDITH BERNER,[a] MARIA FREDIANI,[a] JASON A. OTKIN,[b] AND SARAH M. GRIFFIN[b]

[a] *National Center for Atmospheric Research, Boulder, Colorado*
[b] *Cooperative Institute for Meteorological Satellite Studies, University of Wisconsin–Madison, Madison, Wisconsin*

(Manuscript received 9 March 2020, in final form 25 November 2020)

ABSTRACT: Current state-of-the art regional numerical weather forecasts are run at horizontal grid spacings of a few kilometers, which permits medium- to large-scale convective systems to be represented explicitly in the model. With the convection parameterization no longer active, much uncertainty in the formulation of subgrid-scale processes moves to other areas such as the cloud microphysical, turbulence, and land surface parameterizations. The goal of this study is to investigate experiments with stochastically perturbed parameters (SPP) within a microphysics parameterization and the model's horizontal diffusion coefficients. To estimate the ''true'' uncertainty due to parameter uncertainty, the magnitudes of the perturbations are chosen as realistically as possible and not with a purposeful intent of maximal forecast impact as some prior work has done. Spatial inhomogeneities and temporal persistence are represented using a random perturbation pattern with spatial and temporal correlations. The impact on the distributions of various hydrometeors, precipitation characteristics, and solar and longwave radiation are quantified for a winter case and a summer case. In terms of upscale error growth, the impact is relatively small and consists primarily of triggering atmospheric instabilities in convectively unstable regions. In addition, small in situ changes with potentially large socioeconomic impacts are observed in the precipitation characteristics such as maximum hail size. Albeit the impact of introducing physically based parameter uncertainties within the bounds of aerosol uncertainties is small, their influence on the solar and longwave radiation balances may still have important implications for global model simulations of future climate scenarios.

KEYWORDS: Cloud parameterizations; Ensembles; Model comparison; Numerical weather prediction/forecasting; Stochastic models

1. Introduction

Current state-of-the art regional forecasts are run at numerical spacings of a few kilometers, which allows for the explicit representation of convection. With the convection scheme no longer active, the uncertainty in the formulation of subgrid-scale processes remains in other areas such as the representation of the surface and planetary boundary layer and cloud microphysical processes. While the former plays an essential role in the convective initiation, the latter often determines the properties of clouds, precipitating hydrometeors and the amount of radiation that reaches the ground.

A long-standing problem of ensemble prediction systems is that they are underdispersive, i.e., that the verifying analysis frequently lies outside the uncertainty predicted by the ensemble members. A major reason has been attributed to model uncertainties (Palmer 2001; Berner et al. 2011, 2017). Uncertainties in the formulation of parameterized processes remain problematic even at convection-permitting resolutions (Bouttier et al. 2012; Romine et al. 2014; Schwartz 2019).

The first generation of parameter perturbation schemes introduced static perturbations; i.e., each ensemble member had a different but fixed parameter (e.g., Murphy et al. 2004; Hacker et al. 2011; Berner et al. 2015; Christensen et al. 2015). A disadvantage of this approach is that each ensemble member has a potentially different bias. Alternatively, the parameters can be varied stochastically; i.e., each parameter is perturbed with a temporally evolving perturbation field (e.g., Bowler et al. 2008, 2009; Ollinaho et al. 2017; Jankov et al. 2017, 2019). This assures that all ensemble members have the same climatology, although their bias can be different from the unperturbed forecast. For best results, the perturbation fields should have both, spatial and temporal correlations (e.g., Buizza et al. 1999; Berner et al. 2009).

Jankov et al. (2017, 2019) used the stochastic pattern generator developed by Berner et al. (2015) to perturb key parameters in the convection and planetary boundary layer scheme. They found a small reduction of biases in near-surface variables. Stanford et al. (2019) applied the same pattern generator to perturb the mass–size relationship for unrimed and partially rimed ice as well as the ice fall speed–size relationship in the P3 bulk microphysics scheme (Morrison and Milbrandt 2015; Milbrandt and Morrison 2016) and noted changes to precipitation timing, maxima, and area.

Here, the same stochastic pattern generator is used to perturb key parameters in the Thompson and Eidhammer (2014; hereafter, TE14) ''aerosol-aware'' microphysics scheme, namely the size spectrum for cloud water, the activation of cloud condensation and ice nuclei and the size spectrum of graupel/hail as described in the next section. Many microphysical processes (e.g., riming and autoconversion) employ empirical relationships to represent average functional properties of particles, which cannot be captured even by going to higher resolution (Stanford et al. 2019). The idea of this research is to place the stochastic

Corresponding author: Gregory Thompson, gthompsn@ucar.edu

DOI: 10.1175/MWR-D-20-0077.1

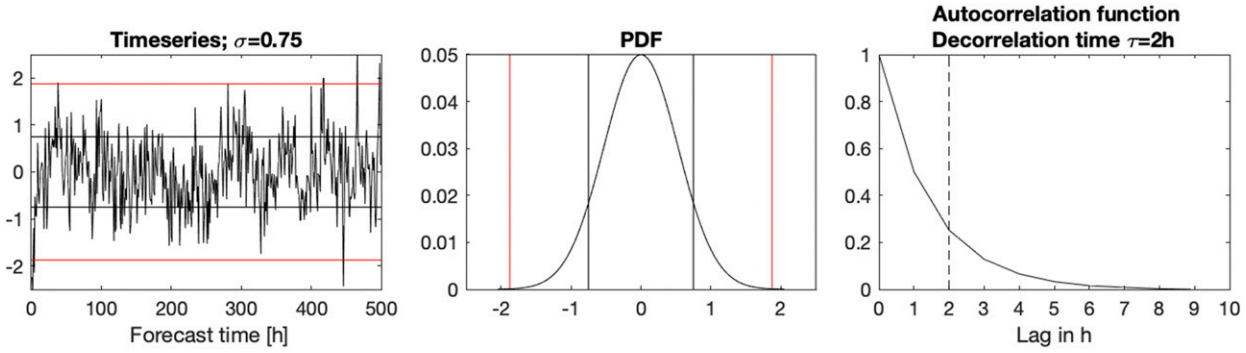

FIG. 1. (a) Realization of perturbation time series at a single grid point, (b) probability distribution function with variance 0.75 and cutoff values of ±2.5, and (c) temporal autocorrelation function.

perturbations as near to the root of uncertainty as possible: within parameters that control microphysical characteristics and/or processes.

This paper presents the implementation details of the *stochastically perturbed parameter* applied to the *microphysics* scheme (SPP-MP) and is organized as follows: section 2 discusses sources of uncertainty in the microphysical processes along with details on the parameter perturbation and the numerical model experiments. Additionally, section 2 describes perturbations using SPP separately to perturb the effective mixing length used within the standard horizontal diffusion scheme (SPP-HDF), while section 3 shows how the stochastic perturbations affect the specific microphysical aspects. The impact of SPP-MP on satellite brightness temperature for two verification periods are reported in a companion paper by Griffin et al. (2020). The relative impacts of the changes by SPP-HDF in comparison to SPP-MP are mentioned along with other primary findings in section 4.

2. Methodology

a. The stochastic pattern generator

The key element of the stochastic pattern generator is that it generates at each time t a two-dimensional random field $r(x, y, t)$ with prescribed spatial and temporal correlations. These, together with an overall amplitude, fully determine the perturbation field.

Assuming the random perturbation field $r(x, y, t)$ in spectral space is given as follows:

$$r(x,y,t) = \sum_{k=-K/2}^{K/2} \sum_{l=-L/2}^{L/2} r_{k,l}(t) e^{2\pi i(kx/X + ly/Y)}, \tag{1}$$

where k and l are the $(K + 1)(L + 1)$ wavenumber components in the zonal x and meridional y directions, respectively; $r_{k,l}$ is the spectral coefficient; and X and Y represent the number of grid points in the x and y directions, respectively. The Fourier modes $e^{2\pi i(kx/X + ly/Y)}$ form an orthogonal set of basis functions on the rectangular domain $0 < x < X$ and $0 < y < Y$. Each spectral coefficient $r_{k,l}$ evolves over time as a first-order autoregressive process:

$$r_{k,l}(t + \Delta t) = \alpha r_{k,l}(t) + g_{k,l}\epsilon_{k,l}. \tag{2}$$

Here, α is the linear autoregressive parameter, $g_{k,l}$ the wavenumber-dependent noise amplitude and $\epsilon_{k,l}$ a Gaussian white-noise process with mean zero and standard deviation one. We note that $r_{k,l}$ contains two terms: 1) a linear autoregressive parameter that is a function of the model time step Δt and a prescribed temporal decorrelation time τ, $\alpha = \exp(-2\Delta t/\tau)$, acting on the previous state and 2) a wavenumber-dependent noise

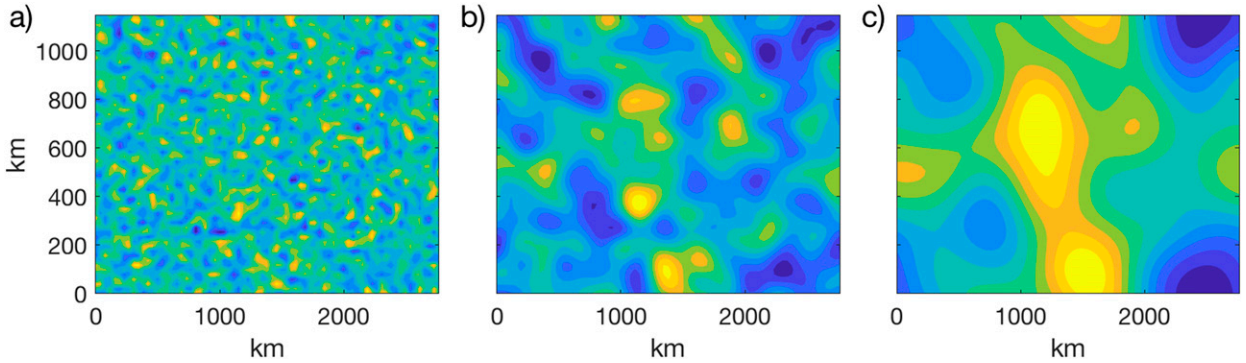

FIG. 2. Example perturbation patterns for three different spatial scales: (a) convection permitting, (b) mesoscale, and (c) synoptic scale.

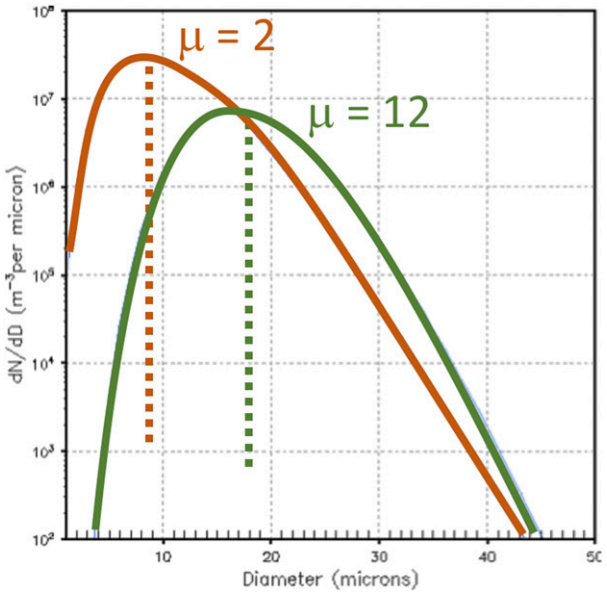

FIG. 3. Number distribution of cloud water drops as a function of diameter (LWC = 0.25 g m^{-3}) using generalized gamma function with shape parameter: $\mu = 2$ (red curve) and $\mu = 12$ (green curve).

amplitude $g_{k,l}$ that is a function of a *prescribed* length scale κ and determines the wavenumber-dependent variance of a Gaussian white-noise process $\varepsilon_{k,l}$:

$$g_{k,l} = F_o e^{-4\pi\kappa\rho_{k,l}^2} \quad \text{with} \quad F_o = \left\{ \frac{\sigma_{k,l}[1-1(1-\alpha)^2]}{2\sum_k \sum_l e^{-8\pi\kappa\rho_{k,l}^2}} \right\}. \tag{3}$$

Here $\rho_{k,l} = (k^2/X^2 + l^2/Y^2)^{1/2}$ is the effective radial wavenumber and $\sigma_{k,l}$ are the spectral variances. The normalization constant F_o is chosen, so that the variance at any grid point, σ^2, is given by the total variance in spectral space.

The scheme is fully determined by three parameters: the temporal decorrelation time τ, the spatial length scale (or spatial decorrelation) κ, and the variance in gridpoint space, σ^2. For the case $\tau = 0$ and $\kappa = 0$, the scheme introduces noise that is white in time and space, with variance σ^2. Therefore, prescribing a temporal decorrelation time and a length scale allows the stochastic perturbations to evolve in time and space with an assigned degree of "memory" (Fig. 1). The result is a stochastically sampled, two-dimensional, time-varying field (Fig. 2) of correlated parameter values that follow locally a Gaussian distribution with a prescribed mean and standard deviation.

b. *Stochastically Perturbed Parameter applied to Microphysics (SPP-MP)*

The TE14 scheme is modified to accept perturbations to three different microphysics aspects. These aspects consist of parameters in the microphysics formulation or in statistical parameters used to represent a bulk distribution. Aspects may be perturbed individually or in combination. Different from

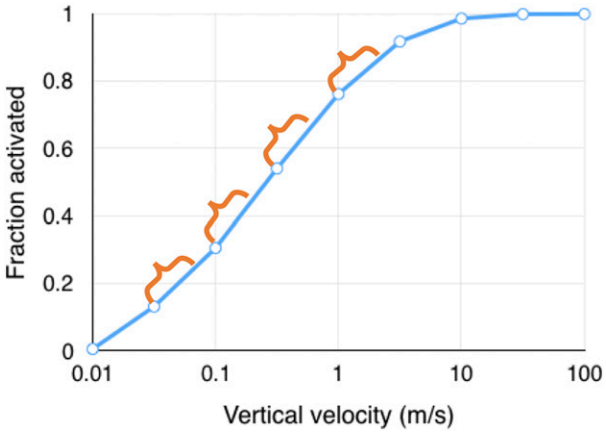

FIG. 4. The fraction of aerosols that activate as CCN as a function of vertical velocity (m s^{-1}). The curly braces provide a visual indication of potential perturbations at four values of vertical velocity.

previous studies (e.g., Hacker et al. 2011; Ollinaho et al. 2017), the aim here is not to conduct sensitivity studies to find the parameters that will have maximal impact but represent true microphysics parameter uncertainty as suggested by observations. The following will discuss rationale for each of the perturbed MP parameters in detail.

1) NUMBER SPECTRUM FOR CLOUD WATER

Within the TE14 scheme, the number spectrum for cloud water is assumed to follow a generalized gamma distribution:

$$N(D) = N_0 D^{\mu} e^{-\lambda D}, \tag{4}$$

where D is the droplet diameter, N_0 is the intercept parameter, μ is the shape parameter, and λ is the distribution slope. Unlike some bulk microphysics schemes that use a constant shape parameter, the TE14 scheme uses a variable μ that is diagnosed at each grid point in space and time based on the predicted cloud droplet number concentration and was designed to match observations from Martin et al. (1994). The current simple diagnosis of μ uses the formula:

$$\mu = \left(\frac{1000}{N_c} + 2 \right), \tag{5}$$

where N_c is the cloud water droplet concentration (cm^{-3}) explicitly predicted by the model and μ is bounded between 2 and 15. The relationship between N_c and μ, however, contains some observational spread and uncertainty (see e.g., Miles et al. 2000). The importance of the variable shape parameter is seen in Fig. 3 with an example liquid water content (LWC) of 0.25 g m^{-3} and two values of the shape parameter: $\mu = 2$ and 12. The larger value of μ for the same LWC results in a larger mean diameter of water drops. In fact, this figure illustrates a case in which the lower value would not be a condition for which rain begins to occur whereas the higher value of μ would initiate the "autoconversion" process in which cloud water converts to rain in the TE14 microphysics scheme. Cloud water would begin to convert to rain in the case of $\mu = 12$ (green curve) since the mean cloud drop size would be larger than

approximately 14 μm whereas the red curve with $\mu = 2$ would not begin forming rain because mean cloud droplet size would be too small ($<10\,\mu$m). For this reason, we choose to introduce uncertainty into this relationship by altering the shape parameter by adding perturbations using the SPP method. Since the predicted onset of rain can be instrumental in many subsequent microphysical processes (e.g., freezing into solid ice/graupel, collection of smaller cloud droplets by accretion, let alone its faster falling velocity to reach the ground as precipitation), having uncertainty related to rain production should be a highly important process worthy of using in this type of experiment.

2) Activation of cloud condensation nuclei (CCN)

Another highly uncertain aspect of the TE14 scheme is the activation of aerosols as cloud droplets and ice crystals. Because there are few in situ observations or routine measurements of aerosols in three-dimensional space, let alone consistent measurements over time, there are large uncertainties in the aerosol number concentration. This, in turn, leads to uncertainty in the number of aerosols that activate into cloud particles. The existing TE14 scheme activates the number of cloud condensation nuclei (CCN) based on a lookup table consisting of vertical updraft strength, temperature, and aerosol characteristics (mean and standard deviation of aerosol diameter as well as the available aerosol concentration). In the current version of the scheme, the model-predicted gridscale vertical velocity is used to retrieve the matching prepopulated updraft strength from the table. However, it is well known that a model's gridscale vertical velocity does not represent the motions of eddies occurring at scales smaller than the grid increment (e.g., Peng et al. 2005).

Figure 4 illustrates the importance of vertical velocity in the activation of aerosols as CCN in the microphysics scheme. The vertical velocity (along with temperature) dictates the supersaturation, which is the dominant factor controlling the number of aerosols that nucleate as cloud droplets. The figure was created by assuming an aerosol concentration of 3000 cm^{-3} at a temperature of 278 K with different updraft strengths shown on the x axis. In this example, if the model's grid-resolved vertical velocity is 0.1 $\mathrm{m\,s}^{-1}$, then 30% of the available aerosols will activate as CCN. However, if the SPP method altered the velocity to 0.3 $\mathrm{m\,s}^{-1}$, then nearly 55% of available aerosols would activate. Thus, nearly double the cloud droplets would exist, which would also affect the final determination of the cloud water spectrum as shown by Eq. (2). It is important to note that the original grid-resolved vertical velocities remains unchanged. The SPP-altered value w' was used to retrieve the activated fraction of aerosols from a lookup table.

In addition to nucleation of aerosols as cloud droplets (i.e., CCN), the TE14 scheme also creates cloud ice crystals from the mineral dust concentration as ice nuclei, or IN. Thus, similar to activating CCN, the controlling factors of temperature and vertical velocity combine to determine the supersaturation and affect the IN and ice crystal concentration; however, unlike the CCN and resulting cloud droplet distribution assumptions, the cloud ice spectra does not use a variable shape parameter μ but instead uses a constant value of zero (inverse exponential distribution).

3) Size spectra of graupel/hail

The third stochastic perturbations applied to the Y-intercept parameter of the graupel/hail size spectrum, thus fundamentally altering the size spectra of the graupel/hail hybrid category. The assumed number density function for this category follows the same generalized gamma distribution of Eq. (1). The Thompson bulk microphysics parameterization was specifically designed to predict only one free variable of a mixed or hybrid graupel/hail category, its mass mixing ratio, in order to reduce computational cost as compared to fully double-moment schemes. One-moment schemes typically assume an inverse-exponential size distribution [$\mu = 0$ in Eq. (1)] with an a priori assigned and constant Y-intercept parameter (N_0). Numerous observations from aircraft and surface measuring campaigns (e.g., McFarquhar and Black 2004; Knight et al. 1982; Field et al. 2019) generally support this distribution shape, although the intercept parameter has been known for decades to vary by as many as two to three orders of magnitude.

Since using a fixed intercept parameter potentially hinders the simulation outcome, we developed a relationship combining graupel mass mixing ratio and amount of supercooled liquid water to compute a space-/time-varying Y-intercept parameter diagnostically during a simulation. From prior observational studies, the intercept parameter is permitted to vary from 10^4 to $10^6\,\mathrm{m}^{-4}$ consistent with overall observations, but the diagnostic relationship itself was ad hoc and not extensively tested. The McFarquhar and Black (2004) observations contradict the scheme's existing diagnostic relation for decreasing intercept parameter as a function of higher graupel mixing ratio; although their observations were collected in tropical storms so their applicability to midlatitude deep convection is unknown. Similar to Fig. 3, the change to graupel Y-intercept parameter effectively changes the size spectra to smaller or larger mean particle size, which has obvious implications to the final maximum hail size to reach the ground.

c. *Stochastically Perturbed Parameter applied to Horizontal Diffusion (SPP-HDF)*

Since the microphysics scheme in numerical models only creates clouds where updrafts are sufficiently cooling the air to condense water vapor into cloud particles, the impacts of SPP-MP are likely to take time to show up in many simulations. However, in certain instances when a convective downdraft (cold pool) produces subsequent low-level convergence and forces adjacent new updraft, its evolution may be altered more rapidly and dramatically due to the graupel Y-intercept perturbations that are responsible for bringing precipitation to the ground more slowly or quickly depending on the perturbation. This scenario, however, represents relatively small areas among a weather forecast covering very large geographic regions. Therefore, we also targeted another part of model uncertainty—the model's horizontal diffusion (mixing) coefficients. Jankov et al. (2019) used the SPP scheme to perturb the MYNN-PBL vertical mixing coefficients, but

TABLE 1. List of stochastically perturbed parameters, spatial and temporal scales, and magnitude.

Aspect perturbed	Spatial length scale (km)	Temporal scale (h)	Magnitude perturbation (for one std dev)
Graupel intercept parameter	200	2	±0.75
Cloud droplet shape parameter	200	2	±2.0
w' used in CCN activation	200	2	+0.375 m s^{-1}
IN concentration	200	2	+13.5×
Horizontal diffusion	50	1	(1 ± 0.2)×

our tests aimed to perturb horizontal mixing in an effort to cause wider impacts to the full domain making new clouds possible to form/dissipate differently than a control experiment. Stanford et al. (2019) also altered the horizontal diffusion in WRF using various static factors, but our effort used a SPP field separate from the one used for SPP-MP to study if changing horizontal diffusion would impact the clouds in larger/smaller ways than SPP-MP.

d. Numerical model experiments

The stochastic pattern generator was configured to have a spatial length scale of 200 km and temporal scale of 2 h to be applicable for typical summertime mesoscale convective complexes in the central United States (Table 1). While the SPP field itself had a standard deviation of 0.75 and cutoff values at ±1.875, these values had to be altered for each of the three aspects discussed in section 2 since they were applied to different physical parameters. Therefore, in application to the graupel intercept parameter, the SPP field was used to offset the $\log_{10}$ of the diagnosed value of Y-intercept parameter. In the case of the cloud water shape parameter, the SPP field was doubled thereby permitting rounded-whole-number changes as large as ±4 in the final diagnosed value. Finally, for the change to CCN activation, the perturbation field was offset by the minimum found on the entire grid then scaled by 1/4 to achieve an absolute maximum of $w' = 0.9375\ \mathrm{m\ s^{-1}}$. To avoid introducing a net downward vertical velocity, which makes no sense for the supersaturation equation, all perturbations of this variable always resulted in increased velocity and CCN activation. The perturbation to IN was a simple multiplication factor of 50 times the SPP random value, which for one standard deviation resulted in 13.5 times more ice crystals, and a maximum factor of nearly 100 times the default number of ice nuclei.

The code changes made within WRF could allow a different perturbation value to be chosen from different vertical levels of a three-dimensional SPP field; however, we applied the same value from the grid's lowest level to each of the three parameters. There is no expectation whatsoever that a specific value used in one aspect internal to the MP scheme would have any physical correlation to the same value perturbing another MP aspect. In other words, perturbing the graupel Y-intercept parameter by an order of magnitude increase has nothing to do with a positive perturbation to the cloud water shape parameter. For the sake of completeness, however, experiments were also run in which each of the three MP aspects were perturbed with different vertical levels of the 3D SPP grid of values; however, no relationships to the outcomes could be determined. We did not perform multiple experiments using different spatial or temporal scales and believe this is potential future work.

Our experiments are based on version 3.9.1.1 of the Weather Research and Forecasting (WRF) Model (Skamarock et al. 2005) configured similar to the High-Resolution Rapid Refresh (HRRR) model (Benjamin et al. 2016). The continental U.S. domain used in our experiments was slightly smaller than the standard HRRR-domain and comprised 1536 × 1024 grid points in the east–west and north–south directions, a 3-km grid spacing, and the same 50 vertical levels as the real-time HRRR model.

The physical parameterization settings were kept similar to the HRRR with the MYNN planetary boundary layer scheme (Nakanishi and Niino 2004), Rapid Radiative Transfer Model for GCMs (RRTMG; Iacono et al. 2000), and the Rapid Update Cycle land surface model (Smirnova et al. 2016). Since the experiments used 3-km grid spacing, no convective parameterization was used. Unlike the operational HRRR, the time step was 15 s and no limit was placed on the microphysical tendencies as is done in the HRRR with its 20-s time step. The simulation design mimics similar simulations to support the annual NOAA Hazardous Weather Testbed Spring Forecasting Experiment (HWT-SFE, e.g., Clark et al. 2012, 2018). Initial condition data for our experiments used the operational Rapid Refresh (RAP) model data (at 13-km spacing) while the lateral boundary conditions used the Global Forecast System (GFS) because our experiments ran for 72-h duration.

Simulations were run with all permutations of the three microphysical aspects as well as a "control" run that omitted the SPP-MP. Table 2 shows the list of experiment names used in upcoming figures and which microphysical aspect was altered in the SPP-MP experiment.

WRF simulations using all aspects of SPP-MP (P7 in Table 2) were initialized at 1200 UTC for 10 days in May 2017

TABLE 2. Experiment names and enabled perturbations.

Expt	Graupel	Cloud water	CCN and IN	Diffusion
Control	No	No	No	No
P1 (G)	Yes	No	No	No
P2 (W)	No	Yes	No	No
P3 (GW)	Yes	Yes	No	No
P4 (A)	No	No	Yes	No
P5 (GA)	Yes	No	Yes	No
P6 (WA)	No	Yes	Yes	No
P7 (GWA)	Yes	Yes	Yes	No
P8 (HDF)	No	No	No	Yes

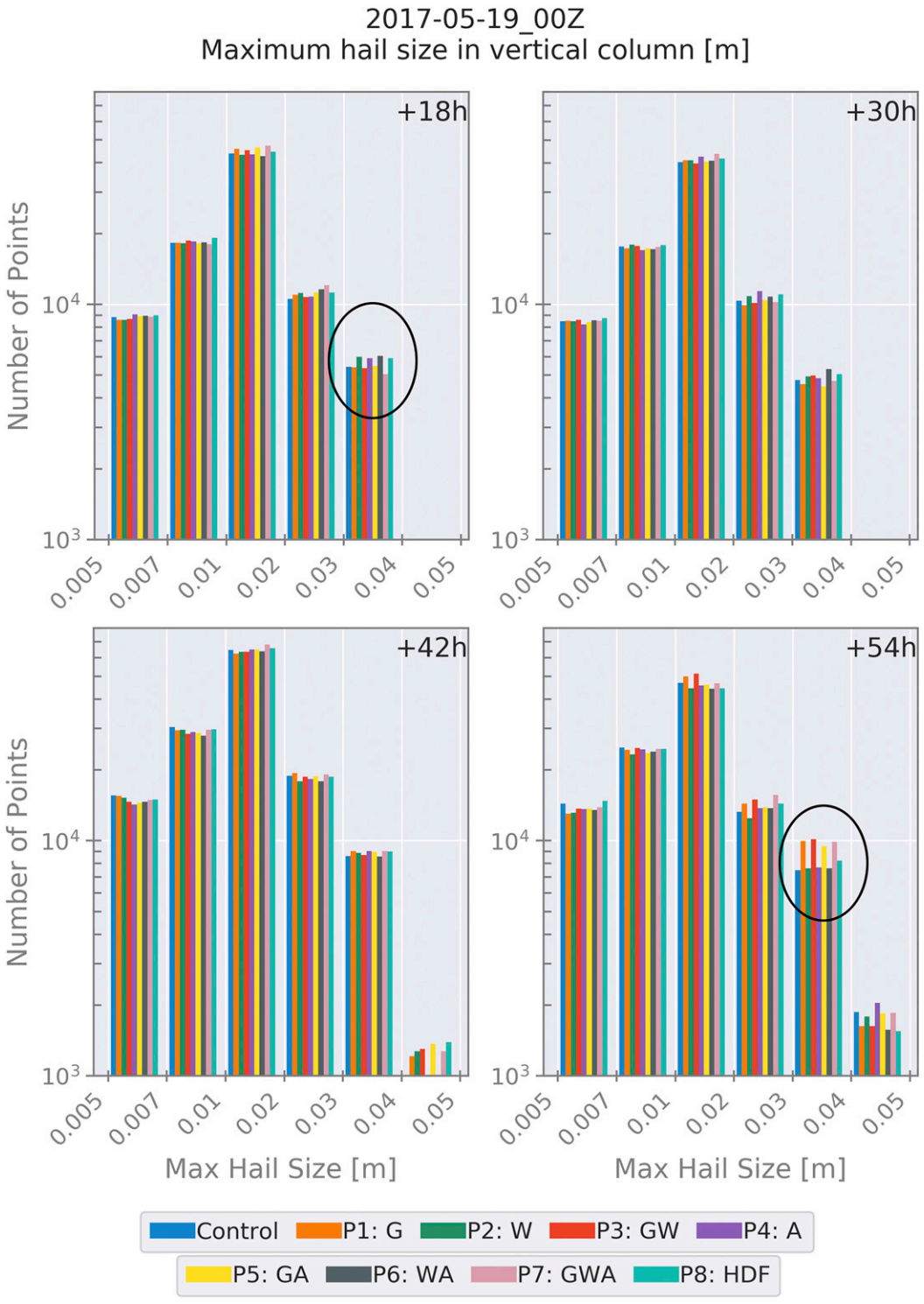

FIG. 5. Histograms of column-maximum graupel/hail size 18, 30, 42, and 54 h for the 19 May 2017 simulation, color coded by sensitivity experiment. Note in particular the 18-h (54-h) forecast shows the experiments with graupel intercept parameter perturbed produced fewer (more) large graupel/hail size.

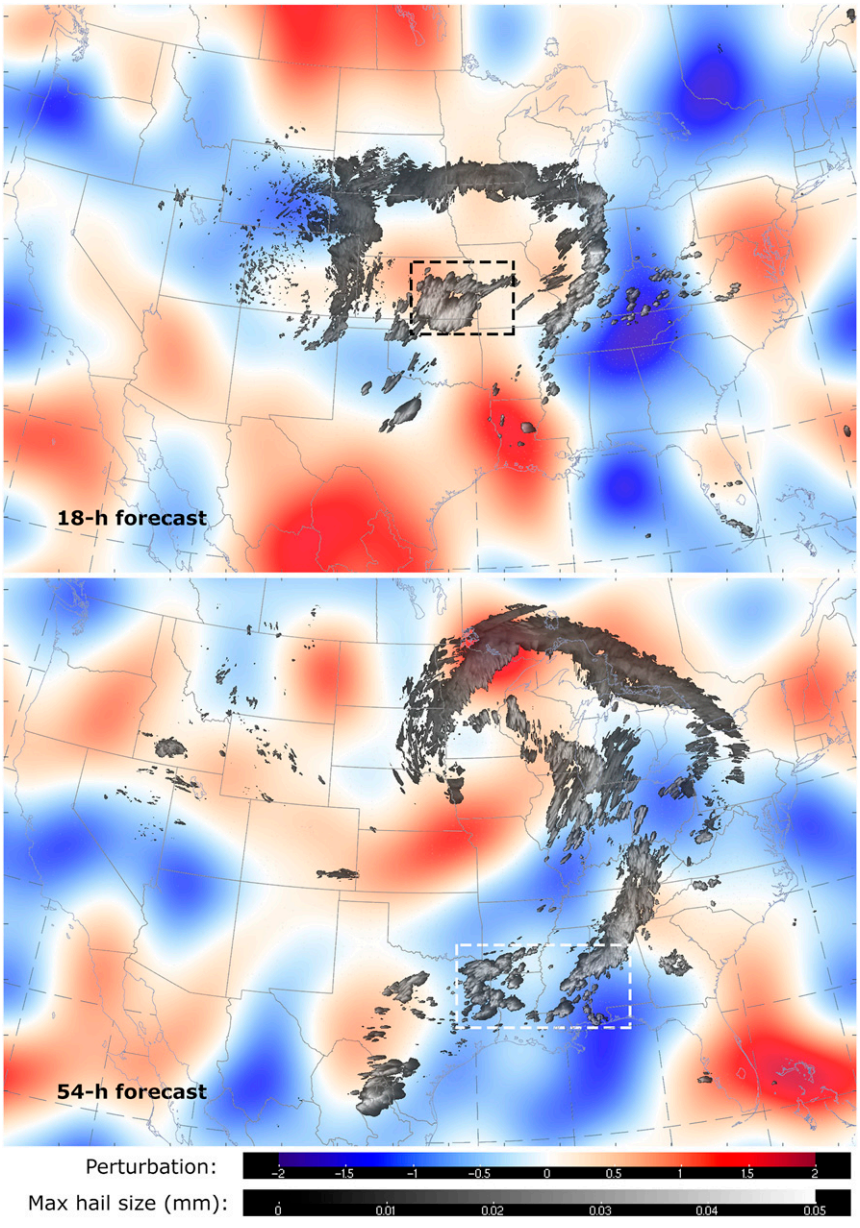

FIG. 6. SPP perturbation pattern (color fill) and maximum-in-column graupel/hail size (m; gray shades) from the (top) 18-h forecast valid at 1800 UTC 19 May 2017 and (bottom) 54-h forecast valid at 0600 UTC 21 May 2017. Boxes outline the regions most responsible for the changes to histograms presented in Fig. 5.

(1, 7, 9, 15, 17, 19, 21, 23, 25, and 27 May) and at 0000 UTC for 10 days in Jan 2018 (7, 9, 11, 13, 19, 21, 23, 25, 27, and 29 January). Validation of WRF forecasts were done in comparison to *GOES-16* satellite data as found in a separate paper by Griffin et al. (2020). This research instead focuses on 2 dates in each set of 10 days because the total number of simulations using seven distinct experiments would be too extreme and unnecessary to show the point of the code alterations. Results discussed in the next section pertain to simulations only on 17 and 19 May 2017 and 11 and 21 January 2018 when synoptic-scale midlatitude cyclones crossed most of the continental United States over a period of 72 h and contained expansive clouds and precipitation. Some of the remaining dates in the set of twenty had less active weather patterns and the chosen dates provide plentiful examples of sensitivities seen in most cases.

3. Results

Given the subtleties of the parameter perturbations as well as the complex interactions between competing and complimentary

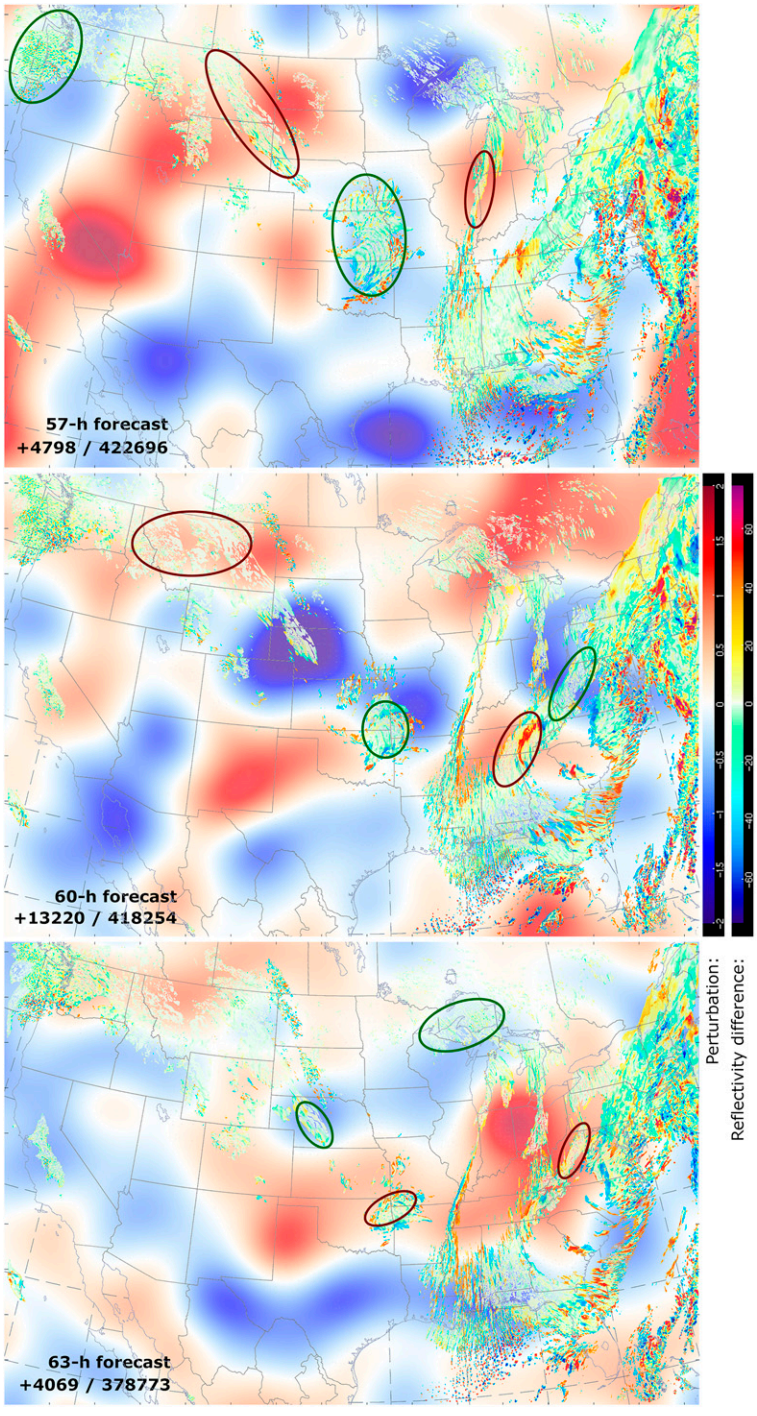

FIG. 7. SPP perturbation pattern (color fill) and radar reflectivity difference (P2 minus control, dBZ) at the model lowest level from the (top) 57 h forecast valid at 0900 UTC 13 Jan 2018, (middle) 60-h forecast valid at 1200 UTC, and (bottom) 63-h forecast valid at 1500 UTC. The dark-red (dark-green) outlined ovals represent areas with correlated increase (decrease) of radar reflectivity and positive (negative) SPP perturbation field. At all three times shown, the number of points with larger reflectivity in the P2 experiment is shown as the first value in the bottom-left corner while the total union of all grid points containing radar reflectivity at the model lowest level is the second value.

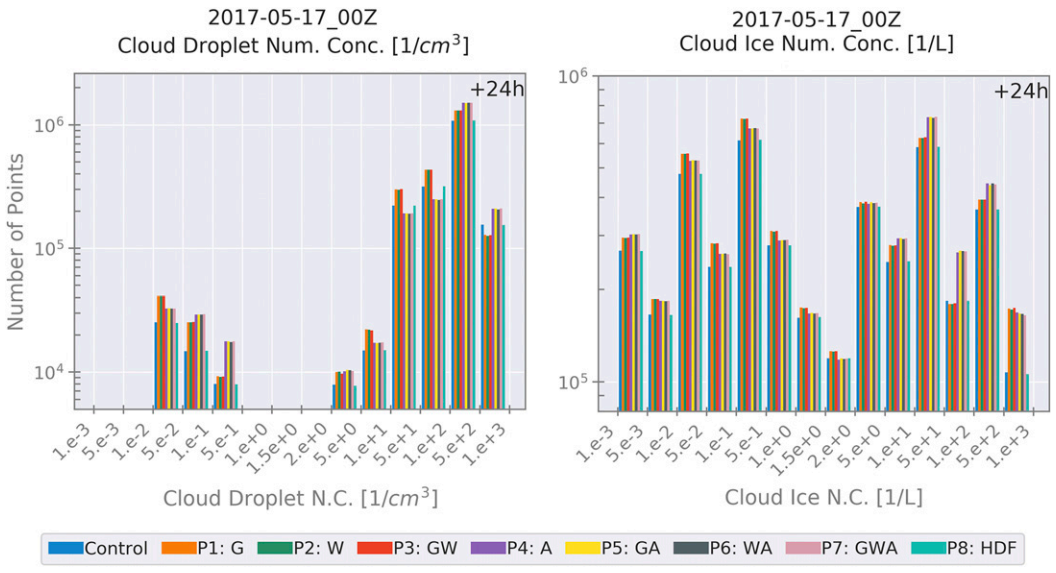

FIG. 8. Histograms of 24-h (left) cloud droplet number concentration and (right) cloud ice number concentration for the WRF sensitivity experiments of 17 May 2017.

microphysical processes in the simulated weather evolution, it is often extremely difficult to pinpoint how the parameter perturbations translate to the expected feedbacks when analyzing the simulation output. Based upon the decisions made to perturb the specific aspects of the MP scheme, some feedbacks to the final forecast should be discernable in the simulations, which is what we discuss in this section.

a. Sensitivity to changing graupel spectra

Since the design of the graupel experiment is to alter the *Y*-intercept parameter of the size spectra of graupel, it should be possible to note the resultant change to a diagnosed maximum size of graupel (or hail). The surface precipitation amount may also be affected by this change; however, due to the relatively small number of grid points that receive graupel at the surface, the change to precipitation is difficult to ascribe directly to the perturbation. Additionally, the numerical effects of "chaos seeding" (Ancell et al. 2018; e.g., their Fig. 4) or, more generally, sensitivity to small perturbations (Lorenz 1963) greatly confound the situation with error growth propagating most rapidly in convective regions to produce completely unphysical responses to minute perturbations. On the other hand, a calculated mean or maximum size of graupel is a more direct response to the characterization of the graupel spectra. In the case of this sensitivity experiment, a *Y*-intercept parameter perturbed to increase (decrease) over the unperturbed value positively implies a smaller (larger) maximum diameter. Therefore, the diagnosed maximum graupel/hail size implemented as in Gagne et al. (2019) was investigated by comparing the control and SPP-MP experiments.

Histograms showing the frequency of WRF grid points containing specific maximum size of graupel/hail were helpful to find the feedback of perturbations as shown in Fig. 5. Note, in particular, that the 18-h forecast reveals a lower frequency of large size graupel/hail in the experiments with perturbed graupel intercept parameter whereas the situation reverses in the 54-h forecast. To trace this feedback to the perturbation field, Fig. 6 presents the 2D SPP field used to perturb the intercept parameter together with the maximum diagnosed particle size as a semitransparent overlay. The boxed regions represent locations with positive (negative) perturbations at forecast hour 18 (54) that leads to smaller (larger) graupel/hail diameter. Although this figure represents one case, it was found very similarly in all four events/dates simulated.

b. Sensitivity to changing cloud water spectra

Sensitivity to the cloud water distribution shape parameter are far more difficult to discern in the results than the graupel spectra changes. The design of perturbing the shape parameter was intended to affect directly the precipitation process of warm rain. The microphysics scheme's way of mimicking the collision–coalescence process in warm rain is through an autoconversion parameterization of cloud to rainwater. The existing MP scheme description of this process is found in Thompson et al. (2004) and follows the original work of Berry and Reinhardt (1974). Increasing (decreasing) the value of the gamma shape parameter shifts the mean size of cloud water larger (smaller) and subsequently promotes (inhibits) warm rain formation. Therefore, investigating the onset of rain through radar reflectivity data was useful to determine if this change produced the desired effect.

Figure 7 shows three consecutive 3-h forecasts from 57 to 63 h of the perturbation field together with an overlay of radar reflectivity difference between P2 experiment and control. Here we can see relatively subtle changes to increase the reflectivity where the perturbations are positive and vice versa. Since the autoconversion process is active at only a very small

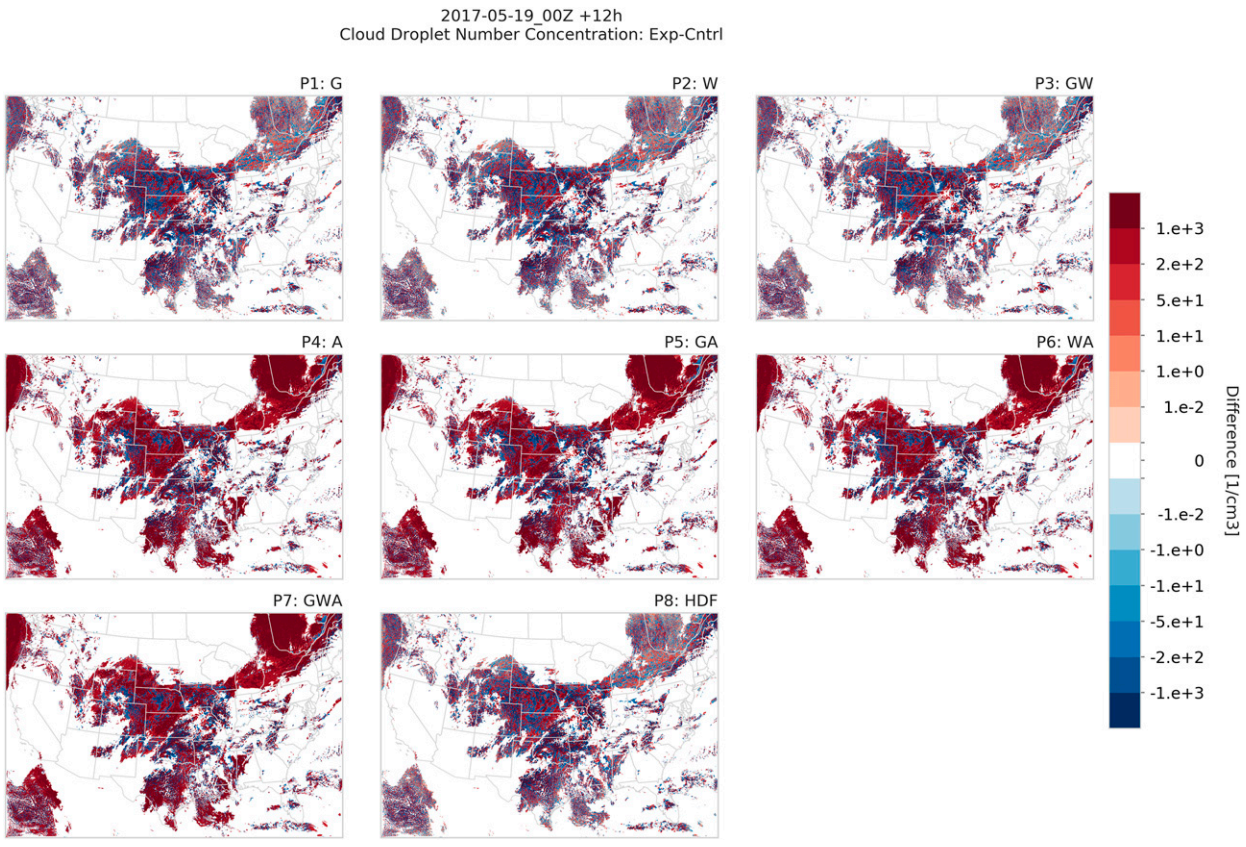

FIG. 9. Difference of column-sum cloud droplet number concentration between each sensitivity experiment and the control. As expected, the concentration is larger in experiments P4–P7 due to the increased CCN activation intended in the experiments while in the remaining experiments it is difficult to see any systematic increase or decrease of droplet concentration.

number of grid points at any simulated instant as well as the fact that the perturbation pattern is ''moving'' through the domain at different rates than the weather systems, it will be difficult to find readily this sensitivity in many other variables.

c. *Sensitivity to changing CCN and IN activation*

The change to cloud condensation and ice nucleation by introducing a positive vertical velocity perturbation to the activation of aerosols produces the largest change found in this study. This is expected since increasing cloud water and ice concentrations of every cloudy point will alter cloud longevity, precipitation formation, radiation, and many other aspects, mostly due to the size changes of cloud water/ice. In other words, for a given value of liquid or ice water content, the additional number of particles directly means that the mean size reduces. There are myriad feedbacks of smaller cloud particles including reduced collection by rain, snow, and graupel (due to lower collection efficiency), inhibition of warm rain (for the reasons mentioned in the previous subsection), and lower terminal velocity.

Figure 8 presents histograms of cloud water and ice number concentrations from the 24-h forecast of the set of 8 experiments and clearly reveals that, as designed, the number of cloud droplets and ice crystals is increased in all experiments where this parameter was perturbed, P4–P7. More subtly, there is a reduction seen in P4–P7 in the lower bins of droplet/ice concentration from the shift produced by the perturbations acting to increase its number.

A more obvious visualization of the difference in cloud droplet number concentration in experiments P4–P7 as compared to P1–P3 is shown in Fig. 9. The vertically integrated number of droplets is clearly increased by the perturbation when activating cloud droplets (and ice). Consequently, the evidence that more numerous cloud droplets inhibits rain formation is found in Fig. 10. The graphic shows the 3-hourly frequency with which each sensitivity experiment had more grid points with 3-hourly rain accumulation higher than the control experiment. Experiments P1–P3 without enhanced CCN and IN nucleation had roughly equivalent number of grid points of 3-h rain amount larger or smaller than the control experiment whereas experiments P4–P7 had significantly more points with less 3-h rain amount. This is a rather clear demonstration of the second aerosol indirect effect as postulated by Albrecht (1989).

Different from the rain amount, the 3-h snow amount was more frequently greater in P4–P7 than control while P1–P3 showed no clear signal in change of snow amount. Prior aerosol–cloud–precipitation studies by Igel et al. (2013) and

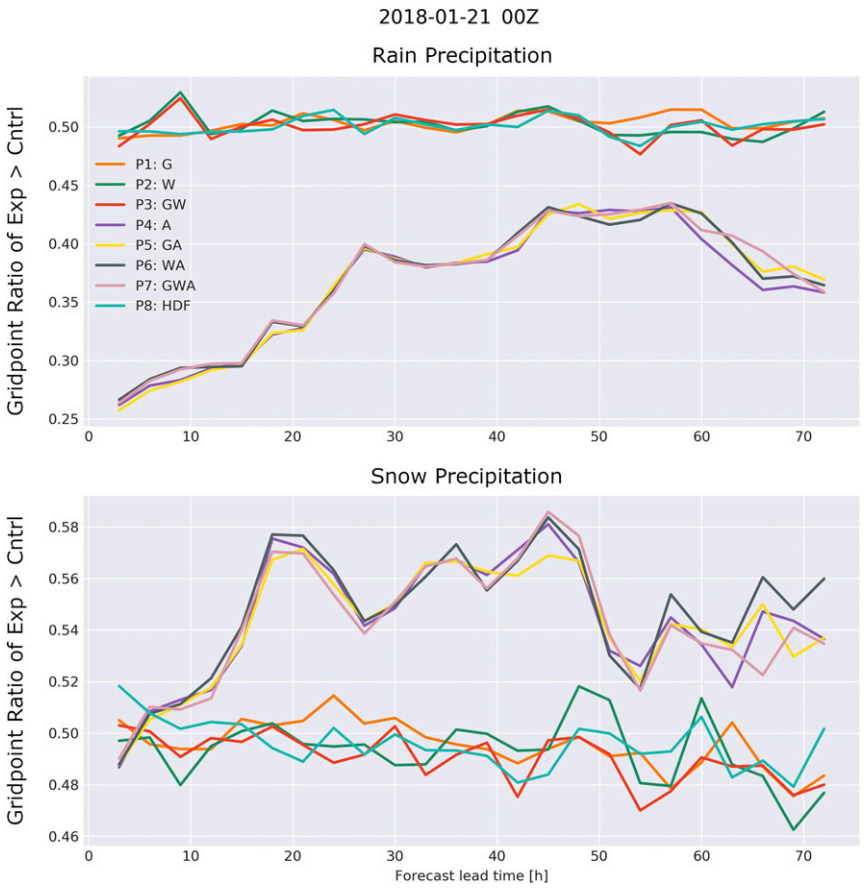

FIG. 10. The frequency of occurrence when (top) rain and (bottom) snow is greater in the sensitivity experiment (P1–P7) as compared to the control experiment. Due to a decrease in overall cloud droplet size in members P4–P7 from activating more CCN and IN, rain formation is hindered, whereas snow is increased.

Thompson and Eidhammer (2014) demonstrated that the more numerous and overall smaller cloud droplet sizes advect farther north of synoptic-scale cyclones and are subsequently captured in the riming process by snow. Our results further confirm this trend and suggest that aerosols can be responsible for precipitation redistribution (also see Lee and Feingold 2010).

The other commonly discussed aerosol indirect effect, frequently called the "albedo effect" following Twomey (1974) is clearly evident in our results. The panels in Fig. 11 show the difference in shortwave radiation reaching the ground in the 18-h forecast valid at 1800 UTC 21 January 2018 from each sensitivity experiment. The increased cloud droplet concentration led to more reflective clouds that lower the amount of shortwave radiation at the ground. In many regions of the synoptic-scale cyclone in this example, the radiation difference between any one experiment and control is more than $-10\,\mathrm{W\,m^{-2}}$, which is roughly an order of magnitude more than suggested by the IPCC (2014) first aerosol indirect effect; although our result is a single time snapshot in a regional model rather than a global long-term simulation average. In combination, the smaller cloud droplet and ice size produces a less efficient precipitation process that results in thicker clouds.

The impact of increasing droplet and ice concentrations is much less obvious in the longwave radiation differences as compared to shortwave radiation as shown in Fig. 12. Here we see mixed results of increased and decreased outgoing longwave radiation at top of the atmosphere. Within regions of widespread high-altitude ice clouds, it appears longwave radiation is decreased, most likely due to the effect of slower-falling ice crystals as would be expected by the shift in mean size of ice; yet in nearby regions there are also increases in longwave radiation suggesting perhaps that liquid clouds are somewhat thicker.

d. Sensitivity to changing horizontal diffusion

To place into context the magnitudes of impacts due to the various perturbations used in SPP-MP, additional experiments were run that altered only the horizontal diffusion coefficients as compared to control while not using SPP-MP. Most of the time, the resulting impacts to the variables previously shown with experiments P1, P2, and P3 were subjectively similar to this HDF experiment. In reviewing graphics of numerous

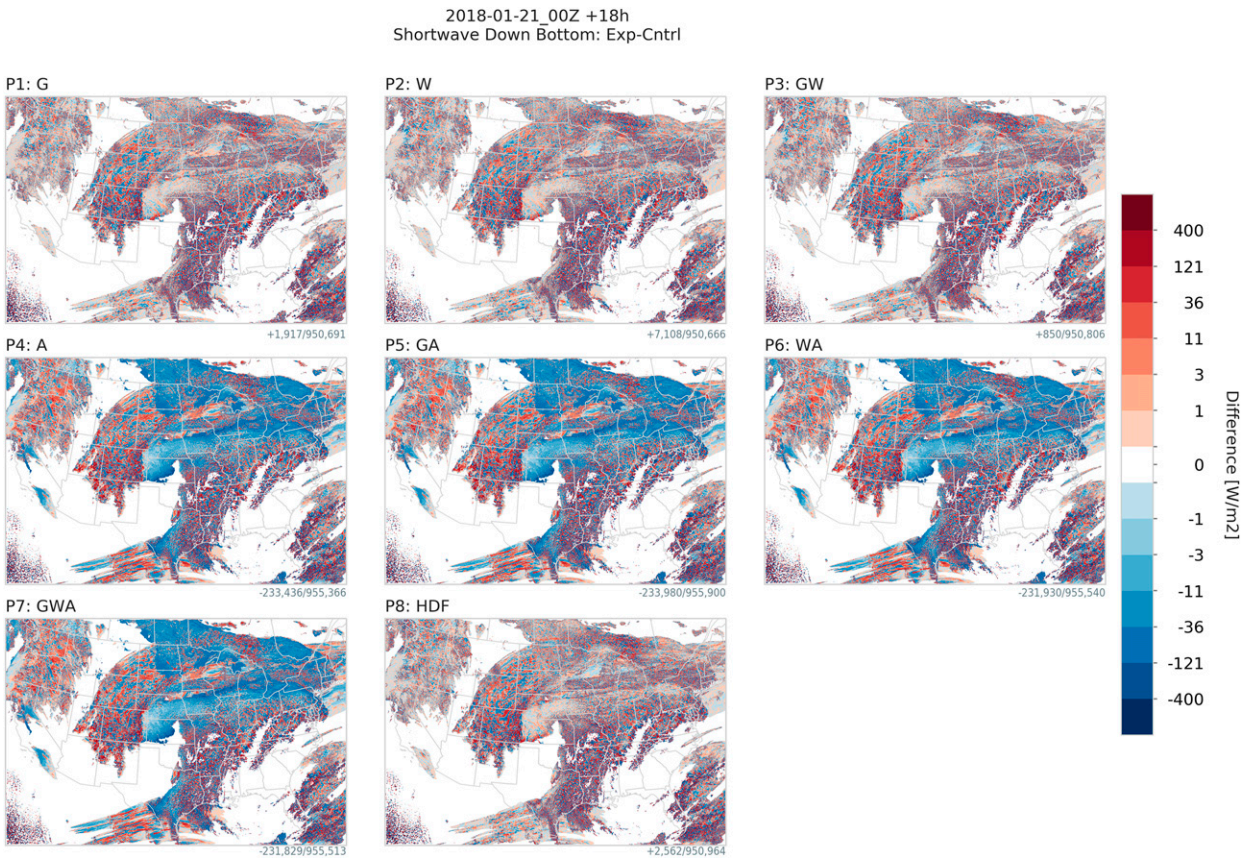

FIG. 11. Difference of shortwave radiation reaching the ground/bottom between each sensitivity experiment and control experiment from the 18-h forecast valid at 1800 UTC 21 Jan 2018. Experiments P1–P3 lack the additional CCN and IN activation and show no systematic change in radiation, whereas experiments P4–P7 have more reflective clouds and show a clear representation of the first aerosol indirect effect (Twomey 1974).

variables from the four 72-h simulations with 3-hourly output, most of the plots showed the same nearly random positive and negative difference patterns that were seen in experiments P1 to P3, even though the time and spatial scales used in the HDF experiment were shorter than the other experiments. Less often, however, the HDF experiment showed more dramatic impacts than SPP-MP in some variables as seen in Figs. 13 and 14.

A principal difference between the HDF and SPP-MP experiments is the fact that changing horizontal diffusion/mixing may alter thermodynamic and kinematic fields sufficiently to cause clouds to either form or dissipate. This is evident in both Figs. 13 and 14 as there are clearly more total grid points that differ for the cloud fraction and shortwave radiation than any of the other seven experiments. There is no possible way to attribute the complete chain of effects from the HDF changes to the production or dissipation of clouds, especially when compounded by the ubiquitous seeding chaos effects (Ancell et al. 2018). The examples displayed in Figs. 13 and 14 contained the most striking examples of differences and even the same day at different forecast times showed much lower impacts. It is postulated that perhaps the periods of strongest synoptic-scale convergence or divergence occurred near the times in the graphics to produce the effects shown here.

4. Discussion and conclusions

In this study we introduced a stochastic parameter perturbation (SPP) scheme that was used to perturb key parameters in an aerosol-aware microphysics scheme (SPP-MP) and in the model's horizontal diffusion coefficients (SPP-HDF). The details for motivating our choices of key parameters and their implementation were described as they were used by Griffin et al. (2020) to study forecast uncertainty in brightness temperature comparisons against *GOES-16* satellite data. The companion paper of Griffin et al. (2020) contained a statistical verification of an ensemble using SPP-MP and showed a relatively minor improvement in spread/skill for a collection of 10 winter cases but not for 10 convective-season cases.

An advantage of SPP is that the perturbations preserve the local conservation properties and physical consistency of the physical parameterization schemes. While some stochastic schemes such as the stochastically perturbed physics tendencies scheme (SPPT) scheme (Palmer et al. 2009; Berner et al. 2015) are tuned to represent missing ensemble spread, we used a "forward" approach and studied the sensitivity to physically justifiable parameter perturbations. One major aspect of this work is to introduce realistic perturbation amplitudes

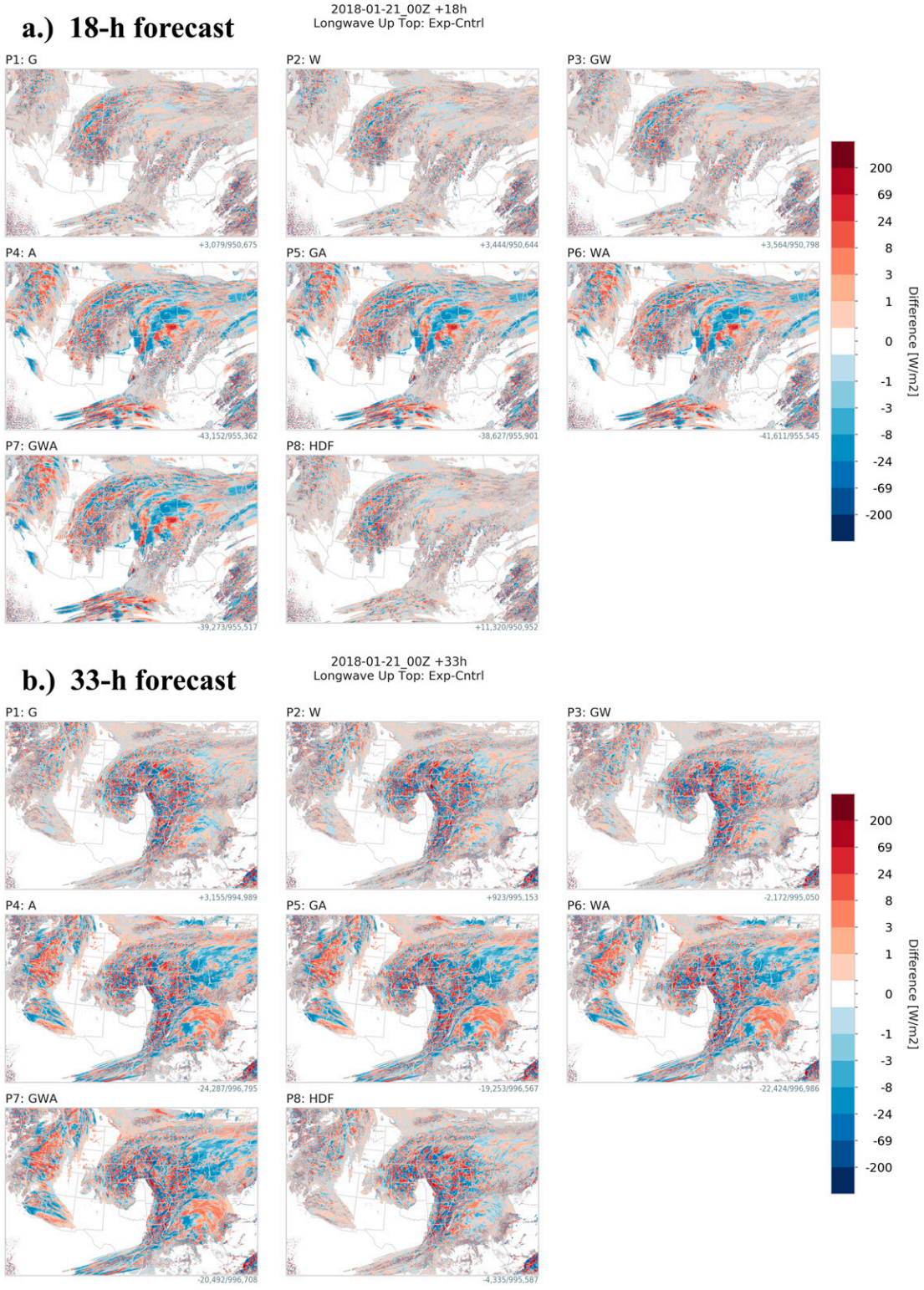

FIG. 12. As in Fig. 11, but for the difference in longwave radiation at the top of the atmosphere between each sensitivity experiment and the control experiment from (a) the 18-h forecast and (b) 15 h later.

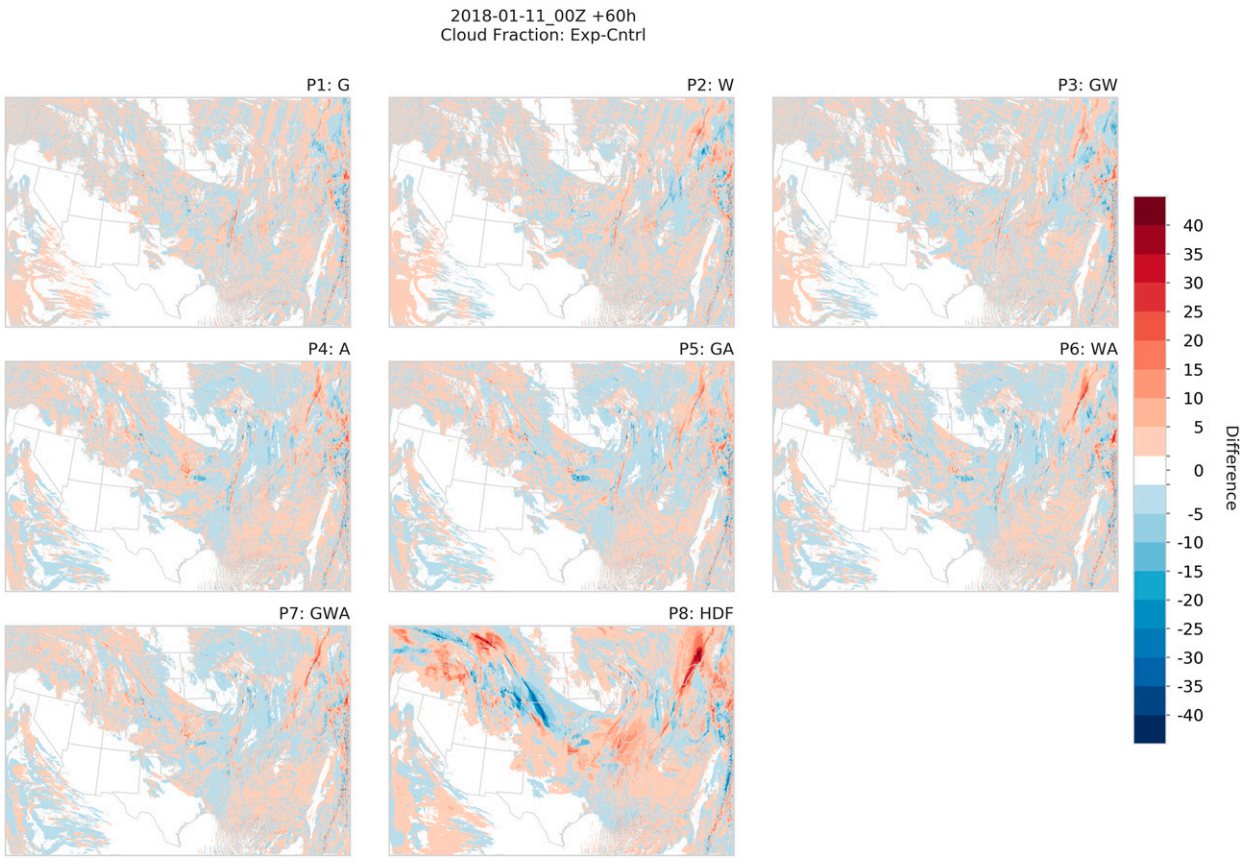

FIG. 13. Difference of vertically integrated cloud fraction between each sensitivity experiment and the control experiment from the 60-h forecast valid at 1200 UTC 13 Jan 2018. Note that experiment P8 (HDF) contains more numerous pixels in total that were affected in addition to showing larger positive and negative shifts of cloud fraction compared to other experiments.

that are informed by "true" parameter uncertainty found in microphysics literature and not unrealistically large amplitude perturbations designed solely to maximize impact. By design all other sources of model error and joint parameter uncertainty between MP and other physical parameterization schemes were not assessed.

A number of simplifying assumptions were used such as the same perturbation pattern being used for all three aspects of MP parameters that were perturbed, thus assuming perfect correlation between the different parameter perturbations. No sensitivity tests to the spatial length or temporal scales were performed. Such tests were performed by Jankov et al. (2019) for SPP applied to the MYNN boundary layer scheme and little sensitivity was reported. Given that the microphysical tendencies are rather intermittent in time and space, we would not expect that a different spatial scale would produce dramatically different outcomes than those presented here. Indeed, we hypothesize that the intermittency of the MP-tendencies is one reason for the relatively small impact of SPP-MP.

Another simplifying assumption was the choice of Gaussian and constant ("barotropic") vertical structure to the SPP pattern to avoid any imbalances in the local conservation properties. However, perturbing the cloud water shape parameter and aerosol activation of water and ice technically represent structural model error as they could affect the vertical structure of clouds.

Based on the limited number of cases studied here, realistic parameter perturbations to the microphysics results in only small upscale error-growth when compared to that needed to improve ensemble dispersion characteristics. The upscale error growth is organized by the flow, in particular convective instabilities, so that the impact of perturbing the horizontal diffusion coefficients led to very similar uncertainty estimates as perturbing the activation of cloud condensation and ice nuclei. This is consistent with previous studies (e.g., Hacker et al. 2011; Berner et al. 2015; Jankov et al. 2017, 2019; Stanford et al. 2019) and can, in part, be remedied by representing uncertainty in other parameterizations schemes, especially the boundary layer scheme and land surface model. Future work is planned to study forecast error spectra in simulations with SPP-MP or parameter perturbations in the PBL to better understand the physical mechanisms of upscale error growth

Locally, the perturbations could have a large impact such as when estimating the uncertainty of extreme weather, e.g., large, damaging hail, and may have substantial socioeconomic benefits in agriculture, aviation, road transportation, etc. An aspect not studied here is that stochastic parameter perturbations have the potential to change the mean state of the climate

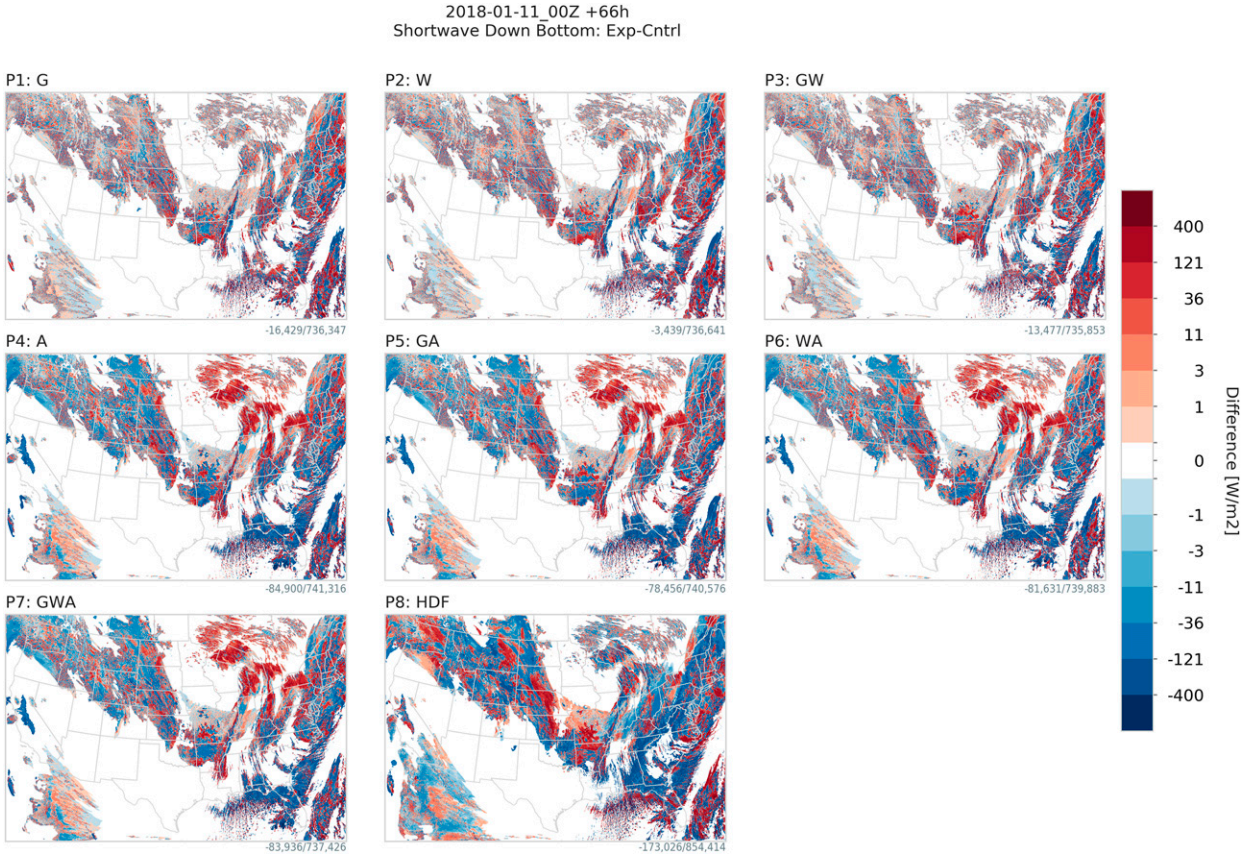

FIG. 14. Difference of shortwave radiation reaching the ground between each sensitivity experiment and the control experiment from the 66-h forecast valid at 1800 UTC 13 Jan 2018. Note that experiment P8 (HDF) reveals increases and reductions of solar radiation differences often much greater than any of the SPP MP experiments

system. (e.g., Lin and Neelin 2000; Berner et al. 2017; Zadra et al. 2018; Palmer 2019). Given the central role of aerosols becoming cloud condensation nuclei for radiative transfer properties, future work should study the role of uncertainties in the formulation of microphysical processes/parameters not only in short-term forecasts, but also in long climate simulations.

Acknowledgments. NCAR is sponsored by the National Science Foundation. We would like to acknowledge high-performance computing support from Cheyenne (doi:10.5065/D6RX99HX) provided by NCAR's Computational and Information Systems Laboratory, sponsored by the National Science Foundation. This project was supported by the NOAA Joint Technology Transfer Initiative (JTTI) via Grants NA17OAR4590179 (UW) and NA17OAR4590171 (NCAR). Additionally, we thank Dr. Hugh Morrison, Mr. McKenna Stanford, and Dr. Joseph Olson for many insightful discussions.

REFERENCES

Albrecht, B. A., 1989: Aerosols, cloud microphysics and fractional cloudiness. *Science*, **245**, 1227–1230, https://doi.org/10.1126/science.245.4923.1227.

Ancell, B. C., A. Bogusz, M. J. Lauridsen, and C. J. Nauert, 2018: Seeding chaos: The dire consequences of numerical noise in NWP perturbation experiments. *Bull. Amer. Meteor. Soc.*, **99**, 615–628, https://doi.org/10.1175/BAMS-D-17-0129.1.

Benjamin, S. G., and Coauthors, 2016: A North American hourly assimilation and model forecast cycle: The Rapid Refresh. *Mon. Wea. Rev.*, **144**, 1669–1694, https://doi.org/10.1175/MWR-D-15-0242.1.

Berner, J., G. Shutts, M. Leutbecher, and T. Palmer, 2009: A spectral stochastic kinetic energy backscatter scheme and its impact on flow-dependent predictability in the ECMWF ensemble prediction system. *J. Atmos. Sci.*, **66**, 603–626, https://doi.org/10.1175/2008JAS2677.1.

——, S.-Y. Ha, J. P. Hacker, A. Fournier, and C. Snyder, 2011: Model uncertainty in a mesoscale ensemble prediction system: Stochastic versus multi-physics representations. *Mon. Wea. Rev.*, **139**, 1972–1995, https://doi.org/10.1175/2010MWR3595.1.

——, K. R. Smith, S.-Y. Ha, J. Hacker, and C. Snyder, 2015: Increasing the skill of probabilistic forecasts: Understanding performance improvements from model-error representations. *Mon. Wea. Rev.*, **143**, 1295–1320, https://doi.org/10.1175/MWR-D-14-00091.1.

——, and Coauthors, 2017: Stochastic parameterization: Toward a new view of weather and climate models. *Bull.*

Amer. Meteor. Soc., **98**, 565–588, https://doi.org/10.1175/BAMS-D-15-00268.1.

Berry, E. X., and R. L. Reinhardt, 1974: An analysis of cloud drop growth by collection. Part II: Single initial distributions. *J. Atmos. Sci.*, **31**, 1825–1831, https://doi.org/10.1175/1520-0469(1974)031<1825:AAOCDG>2.0.CO;2.

Bouttier, F., B. Vié, O. Nuissier, and L. Raynaud, 2012: Impact of stochastic physics in a convection permitting ensemble. *Mon. Wea. Rev.*, **140**, 3706–3721, https://doi.org/10.1175/MWR-D-12-00031.1.

Bowler, N. E., A. Arribas, K. R. Mylne, K. B. Robertson, and S. E. Beare, 2008: The MOGREPS short-range ensemble prediction system. *Quart. J. Roy. Meteor. Soc.*, **134**, 703–722, https://doi.org/10.1002/qj.234.

——, ——, S. E. Beare, K. R. Mylne, and G. J. Shutts, 2009: The local ETKF and SKEB: Upgrades to the MOGREPS short-range ensemble prediction system. *Quart. J. Roy. Meteor. Soc.*, **135**, 767–776, https://doi.org/10.1002/qj.394.

Buizza, R., M. Milleer, and T. N. Palmer, 1999: Stochastic representation of model uncertainties in the ECMWF ensemble prediction system. *Quart. J. Roy. Meteor. Soc.*, **125**, 2887–2908, https://doi.org/10.1002/qj.49712556006.

Christensen, H. M., I. M. Moroz, and T. N. Palmer, 2015: Stochastic and perturbed parameter representations of model uncertainty in convection parameterization. *J. Atmos. Sci.*, **72**, 2525–2544, https://doi.org/10.1175/JAS-D-14-0250.1.

Clark, A. J., and Coauthors, 2012: An overview of the 2010 Hazardous Weather Testbed Experimental Forecasting Program Spring Experiment. *Bull. Amer. Meteor. Soc.*, **93**, 55–74, https://doi.org/10.1175/BAMS-D-11-00040.1.

——, and Coauthors, 2018: The Community Leveraged Unified Ensemble (CLUE) in the 2016 NOAA/Hazardous Weather Testbed Spring Forecasting Experiment. *Bull. Amer. Meteor. Soc.*, **99**, 1433–1448, https://doi.org/10.1175/BAMS-D-16-0309.1.

Field, P. R., A. J. Heymsfield, A. G. Detwiler, and J. M. Wilkinson, 2019: Normalized hail particle size distribution from the T-28 storm-penetrating aircraft. *J. Appl. Meteor. Climatol.*, **58**, 231–245, https://doi.org/10.1175/JAMC-D-18-0118.1.

Gagne, D. J., II, S. E. Haupt, D. W. Nychka, and G. Thompson, 2019: Interpretable deep learning for spatial analysis of severe hailstorms. *Mon. Wea. Rev.*, **147**, 2827–2845, https://doi.org/10.1175/MWR-D-18-0316.1.

Griffin, S. M., J. A. Otkin, G. Thompson, M. Frediani, J. Berner, and F. Kong, 2020: Assessing the impact of stochastic perturbations in cloud microphysics using *GOES-16* infrared brightness temperatures. *Mon. Wea. Rev.*, **148**, 3111–3137, https://doi.org/10.1175/MWR-D-20-0078.1.

Hacker, J. P., C. Snyder, S.-Y. Ha, and M. Pocernich, 2011: Linear and nonlinear response to parameter variations in a mesoscale model. *Tellus*, **63A**, 429–444, https://doi.org/10.1111/j.1600-0870.2010.00505.x.

Iacono, M. J., E. J. Mlawer, S. A. Clough, and J.-J. Morcrette, 2000: Impact of an improved longwave radiation model, RRTM, on the energy budget and thermodynamic proper—Ties of the NCAR Community Climate Model, CCM3. *J. Geophys. Res.*, **105**, 14 873–14 890, https://doi.org/10.1029/2000JD900091.

Igel, A. L., S. C. van den Heever, C. M. Naud, S. M. Saleeby, and D. J. Posselt, 2013: Sensitivity of warm-frontal processes to cloud-nucleating aerosol concentrations. *J. Atmos. Sci.*, **70**, 1768–1783, https://doi.org/10.1175/JAS-D-12-0170.1.

IPCC, 2014: *Climate Change 2014: Synthesis Report*. Cambridge University Press, 151 pp.

Jankov, I., and Coauthors, 2017: A performance comparison between multiphysics and stochastic approaches within a North American RAP ensemble. *Mon. Wea. Rev.*, **145**, 1161–1179, https://doi.org/10.1175/MWR-D-16-0160.1.

——, J. Beck, J. Wolff, M. Harrold, J. B. Olson, T. Smirnova, C. Alexander, and J. Berner, 2019: Stochastically perturbed parameterizations in an HRRR-based ensemble. *Mon. Wea. Rev.*, **147**, 153–173, https://doi.org/10.1175/MWR-D-18-0092.1.

Knight, C. A., W. A. Cooper, D. W. Breed, I. R. Paluch, P. L. Smith, and G. Vali, 1982: Microphysics. *Hailstorms of the Central High Plains*, *Vol. 1. The National Hail Research Experiment*, C. A. Knight, and P. Squires, Eds., Associated University Press, 151–193.

Lee, S.-S., and G. Feingold, 2010: Precipitating cloud-system response to aerosol perturbations. *Geophys. Res. Lett.*, **37**, L23806, https://doi.org/10.1029/2010GL045596.

Lin, J. W. B., and J. D. Neelin, 2000: Influence of a stochastic moist convective parameterization on tropical climate variability. *Geophys. Res. Lett.*, **27**, 3691–3694, https://doi.org/10.1029/2000GL011964.

Lorenz, E. N., 1963: Deterministic nonperiodic flow. *J. Atmos. Sci.*, **20**, 130–141, https://doi.org/10.1175/1520-0469(1963)020<0130:DNF>2.0.CO;2.

Martin, G. M., D. W. Johnson, and A. Spice, 1994: The measurement and parameterization of effective radius of droplets in warm stratocumulus clouds. *J. Atmos. Sci.*, **51**, 1823–1842, https://doi.org/10.1175/1520-0469(1994)051<1823:TMAPOE>2.0.CO;2.

McFarquhar, G. M., and R. A. Black, 2004: Observations of particle size and phase in tropical cyclones: Implications for mesoscale modeling of microphysical processes. *J. Atmos. Sci.*, **61**, 422–439, https://doi.org/10.1175/1520-0469(2004)061<0422:OOPSAP>2.0.CO;2.

Milbrandt, J. A., and H. Morrison, 2016: Parameterization of cloud microphysics based on the prediction of bulk ice particle properties. Part III: Introduction of multiple free categories. *J. Atmos. Sci.*, **73**, 975–995, https://doi.org/10.1175/JAS-D-15-0204.1.

Miles, N. L., J. Verlinde, and E. E. Clothiaux, 2000: Cloud droplet size distributions in low-level stratiform clouds. *J. Atmos. Sci.*, **57**, 295–311, https://doi.org/10.1175/1520-0469(2000)057<0295:CDSDIL>2.0.CO;2.

Morrison, H., and J. A. Milbrandt, 2015: Parameterization of cloud microphysics based on the prediction of bulk ice particle properties. Part I: Scheme description and idealized tests. *J. Atmos. Sci.*, **72**, 287–311, https://doi.org/10.1175/JAS-D-14-0065.1.

Murphy, J., D. Sexton, D. Barnett, G. Jones, M. Webb, M. Collins, and D. Stainforth, 2004: Quantification of modelling uncertainties in a large ensemble of climate change simulations. *Nature*, **430**, 768–772, https://doi.org/10.1038/nature02771.

Nakanishi, M., and H. Niino, 2004: An improved Mellor–Yamada level-3 model with condensation physics: Its design and verification. *Bound.-Layer Meteor.*, **112**, 1–31, https://doi.org/10.1023/B:BOUN.0000020164.04146.98.

Ollinaho, P., and Coauthors, 2017: Towards process-level representation of model uncertainties: Stochastically perturbed parametrizations in the ECMWF ensemble. *Quart. J. Roy. Meteor. Soc.*, **143**, 408–422, https://doi.org/10.1002/qj.2931.

Palmer, T. N., 2001: A nonlinear dynamical perspective on model error: A proposal for non-local stochastic-dynamic parametrization in weather and climate prediction models. *Quart.*

J. Roy. Meteor. Soc., **127**, 279–304, https://doi.org/10.1002/qj.49712757202.

——, 2019: Stochastic weather and climate models. *Nat. Rev. Phys.*, **1**, 463–471, https://doi.org/10.1038/S42254-019-0062-2.

——, R. Buizza, F. Doblas-Reyes, T. Jung, M. Leutbecher, G. J. Shutts, M. Steinheimer, and A. Weisheimer, 2009: Stochastic parametrization and model uncertainty. ECMWF Tech. Memo. 598, 44 pp., https://www.ecmwf.int/sites/default/files/elibrary/2009/11577-stochastic-parametrization-and-model-uncertainty.pdf.

Peng, Y., U. Lohmann, and R. Leaitch, 2005: Importance of vertical velocity variations in the cloud droplet nucleation process of marine stratus clouds. *J. Geophys. Res.*, **110**, D21213, https://doi.org/10.1029/2004JD004922.

Romine, G. S., C. S. Schwartz, J. Berner, K. R. Smith, C. Snyder, J. L. Anderson, and M. L. Weisman, 2014: Representing forecast error in a convection-permitting ensemble system. *Mon. Wea. Rev.*, **142**, 4519–4541, https://doi.org/10.1175/MWR-D-14-00100.1.

Schwartz, C. S., 2019: Medium-range convection-allowing ensemble forecasts with a variable-resolution global model. *Mon. Wea. Rev.*, **147**, 2997–3023, https://doi.org/10.1175/MWR-D-18-0452.1.

Skamarock, W. C., J. B. Klemp, J. Dudhia, D. O. Gill, D. M. Barker, W. Wang, and J. G. Powers, 2005: A description of the Advanced Research WRF version 2. NCAR Tech. Note NCAR/TN-468+STR, 88 pp., https://doi.org/10.5065/D6DZ069T.

Smirnova, T. G., J. M. Brown, S. G. Benjamin, and J. S. Kenyon, 2016: Modifications to the Rapid Update Cycle Land Surface Model (RUC LSM) available in the Weather Research and Forecasting (WRF) Model. *Mon. Wea. Rev.*, **144**, 1851–1865, https://doi.org/10.1175/MWR-D-15-0198.1.

Stanford, M. W., H. Morrison, A. Varble, J. Berner, W. Wu, G. McFarquhar, and J. A. Milbrandt, 2019: Sensitivity of simulated deep convection to a stochastic ice microphysics framework. *J. Adv. Model. Earth Syst.*, **11**, 3362–3389, https://doi.org/10.1029/2019MS001730.

Thompson, G., and T. Eidhammer, 2014: A study of aerosol impacts on clouds and precipitation development in a large winter cyclone. *J. Atmos. Sci.*, **71**, 3636–3658, https://doi.org/10.1175/JAS-D-13-0305.1.

——, R. M. Rasmussen, and K. Manning, 2004: Explicit forecasts of winter precipitation using an improved bulk microphysics scheme. Part I: Description and sensitivity analysis. *Mon. Wea. Rev.*, **132**, 519–542, https://doi.org/10.1175/1520-0493(2004)132<0519:EFOWPU>2.0.CO;2.

Twomey, S., 1974: Pollution and the planetary albedo. *Atmos. Environ.*, **8**, 1251–1256, https://doi.org/10.1016/0004-6981(74)90004-3.

Zadra, A., and Coauthors, 2018: Systematic errors in weather and climate models: Nature, origins, and way forward. *Bull. Amer. Meteor. Soc.*, **99**, ES67–ES70, https://doi.org/10.1175/BAMS-D-17-0287.1.